Fuel 255 (2019) 115850

Contents lists available at ScienceDirect

Fuel

journal homepage: www.elsevier.com/locate/fuel

Full Length Article

Experimental study of the phase behavior of methane and crude oil mixtures

José Francisco Romero Yanes[a], Filipe Xavier Feitosa[a], Felipe Pereira Fleming[b], Hosiberto Batista de Sant'Ana[a,*]

[a] Grupo de Pesquisa em Termofluidodinâmica Aplicada, Chemical Engineering Department, Universidade Federal do Ceará, Fortaleza, CE, Brazil
[b] CENPES – Centro de Pesquisa e Desenvolvimento Leopoldo Américo de Mello, Cidade Universitária, Rio de Janeiro, RJ, Brazil

ARTICLE INFO

Keywords:
PVT
Phase behavior
Asphaltenes
Precipitation

ABSTRACT

Phase behavior of reservoir fluids is crucial for an efficient production development project. In this paper, a new dataset of phase transitions of Brazilian pre-salt crude oil mixed with methane systems is presented and phase behavior discussed under different analytical technics. A series of mixtures of a dead crude (API 28.0, 0.68 wt% of asphaltenes) with 65.0, 67.5, 70.0, 72.5, and 75.0 mol% of methane were studied by constant mass expansion in a PVT cell, coupled with a high-pressure microscopy (HPM). Pressure-volume data shows slight phase transition, with a not evident break due to difference on compressibility, specially by increasing methane molar content. For this reason, beside of visual observation, a near-infrared (NIR) transmittance was used for a proper identification of bubble point pressure. NIR transmittance also allow the detection of phase transitions above bubble point, that was confirmed by intermediate of by HPM analysis. A dispersion of fine particles was detected, and it was associated with asphaltenes onset, for the systems with high content of gas (72.5 and 75.0 mol% of methane). NIR transmittance along with micrographs taken during system pressurization confirm a low asphaltene hysteresis redissolution, with no flocs and mayor aggregates formation and rapid redissolution after system pressurization. This phenomenon could be related to the low content of asphaltenes on the crude oil sample.

1. Introduction

Understanding the phase behavior of petroleum fluids under reservoir and production conditions are essential for a robust and efficient production development project [1,2]. Complex multiphase equilibria may occur as reservoir fluid undergoes condition changes during production or due to composition changes during enhanced oil recovery EOR schemes [3,4]. Light end hydrocarbons (natural gas, propane, etc.), carbon dioxide and nitrogen are used for reservoir gas flooding, contributing to changes in reservoir composition and phase transitions [3,5].

Complex equilibria have been reported in the literature for crude oil and gases systems, including methane [6,7], ethane[7], carbon dioxide [8–10], and high carbon number solvents [4,11–13]. Liquid-vapor, liquid-liquid, and solid-liquid boundaries are important phenomena [5,14–16] specially for crude oils with asphaltenes precipitation [11,12,15].

Asphaltenes are commonly identified as the heaviest and the most polar group of crude oil components [17], and its precipitation is normally associated with changes in pressure [18], temperature [19,20], and compositional variations in the crude oil [5,21–23]. These changes are crucial specially during crude oil production. Injection of miscible low molecular weight gases, e.g., carbon dioxide or natural gas, can also lead to asphaltenes destabilization and precipitation [9,24], and the precipitation extent has been related with gas to oil ratio, gas composition and crude oil properties [25].

Destabilization and precipitation of asphaltenes could affect permanently well production by forming hardly-to-remove deposits in the wellbore area, reservoir formation, pipes and production equipment [15,26]. Reversibility of asphaltenes is a matter under relevant discussion in the literature, for experimental or modeling purpose, specially under reservoir conditions [27,28]. Solubility models [29,30] use thermodynamic phase behavior to describe the asphaltene precipitation, treating it as a reversible phase transition. In the other hand, colloidal models [31,32] supports that asphaltenes are stabilized by resins and maltene fractions, and after asphaltenes destabilization there is an irreversible precipitation process.

Moreover, asphaltenes precipitation and redissolution has being described as a slow kinetic process [27,28,33,34], especially for complex oils and for asphaltenes precipitation by adding n-alkanes [33,35].

* Corresponding author.
E-mail address: hbs@ufc.br (H.B. de Sant'Ana).

https://doi.org/10.1016/j.fuel.2019.115850
Received 25 January 2019; Received in revised form 11 April 2019; Accepted 18 July 2019
Available online 24 July 2019

Table 1
Density, average molar weigh and SARA analysis for the dead crude.

Crude oil properties	
API gravity, °API	28.0
density at 40 °C, kg/m^3	889.1
average molar weight, kg/kmol	250
saturates content ± 1, wt%	59
aromatic content ± 1, wt%	22
resins content ± 1, wt%	18
asphaltenes content ± 0.05, wt%	0.68
water content, wt%	0.49

Table 2
Compositional analysis of the dead crude oil.

Carbon number	wt %	mol %
C3	0.00	0.00
iC4	0.01	0.04
nC4	0.06	0.28
iC5	0.13	0.53
nC5	0.27	1.10
C6	0.95	3.31
C7	2.15	6.51
C8	3.09	8.43
C9	2.90	6.98
C10	2.58	5.61
C11	2.47	4.91
C12	2.35	4.26
C13	2.68	4.47
C14	2.41	3.70
C15	2.55	3.61
C16	2.09	2.74
C17	2.04	2.51
C18	2.23	2.59
C19	2.10	2.33
C20+	66.93	36.09
C20+ molar weight	541	

Asphaltenes precipitation reversibility have been also correlated to asphaltenes source, i.e., petroleum properties; and, operational conditions after asphaltenes precipitation onset [27,33,36]. It has been discussed in the literature [27] that there is a hysteresis between

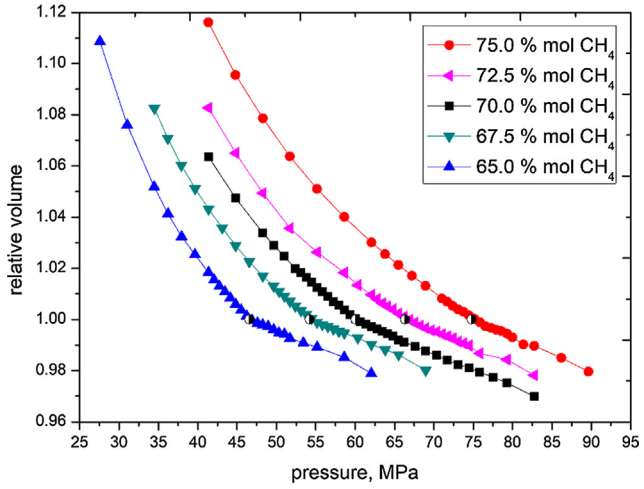

Fig. 2. Relative volume and saturation pressures (◑) of crude oil and methane systems during CCE depletions.

asphaltenes precipitation and redissolution process by compression. Some of the phenomenological conclusions depends on the experimental observations of asphaltene precipitation and saturation envelope [37]. It is important to note that there is a lack of experimental data reporting this phase transition covering a wide range of operational condition for reservoir fluids in the literature.

From an industrial perspective, studies of mixtures of specific gases or solvents with crude oil, is a common practice to identify solubility effects of each solvent over the heavy and complicated fractions of the crude oil, i.e., asphaltenes [4,5,9,38]. Most of the literature data in mixtures of methane or natural gas with crude oil shows an identification of the phase boundaries, i.e., bubble point pressure and asphaltene onset pressure, specially used to fit models' parameters, validate phase behavior's predictive methods, and the further calculation of derivative thermodynamic properties [5,39,40]. Nevertheless, characteristics of the phase transitions for these systems is scarce in open literature, especially for asphaltenes and related equilibria at higher pressures than the bubble pressure point [41]. In this sense, the present work aims to contribute to the analysis and understanding of phase transitions' characteristics for the systems of methane and crude oil,

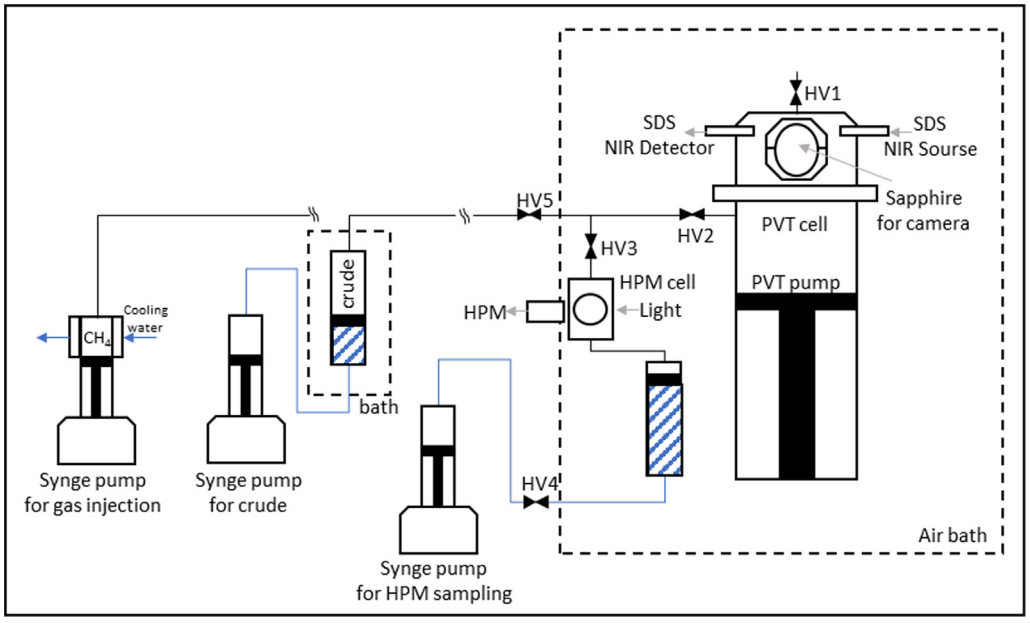

Fig. 1. Schematic diagram of PVT, HPM and sample injection ensemble.

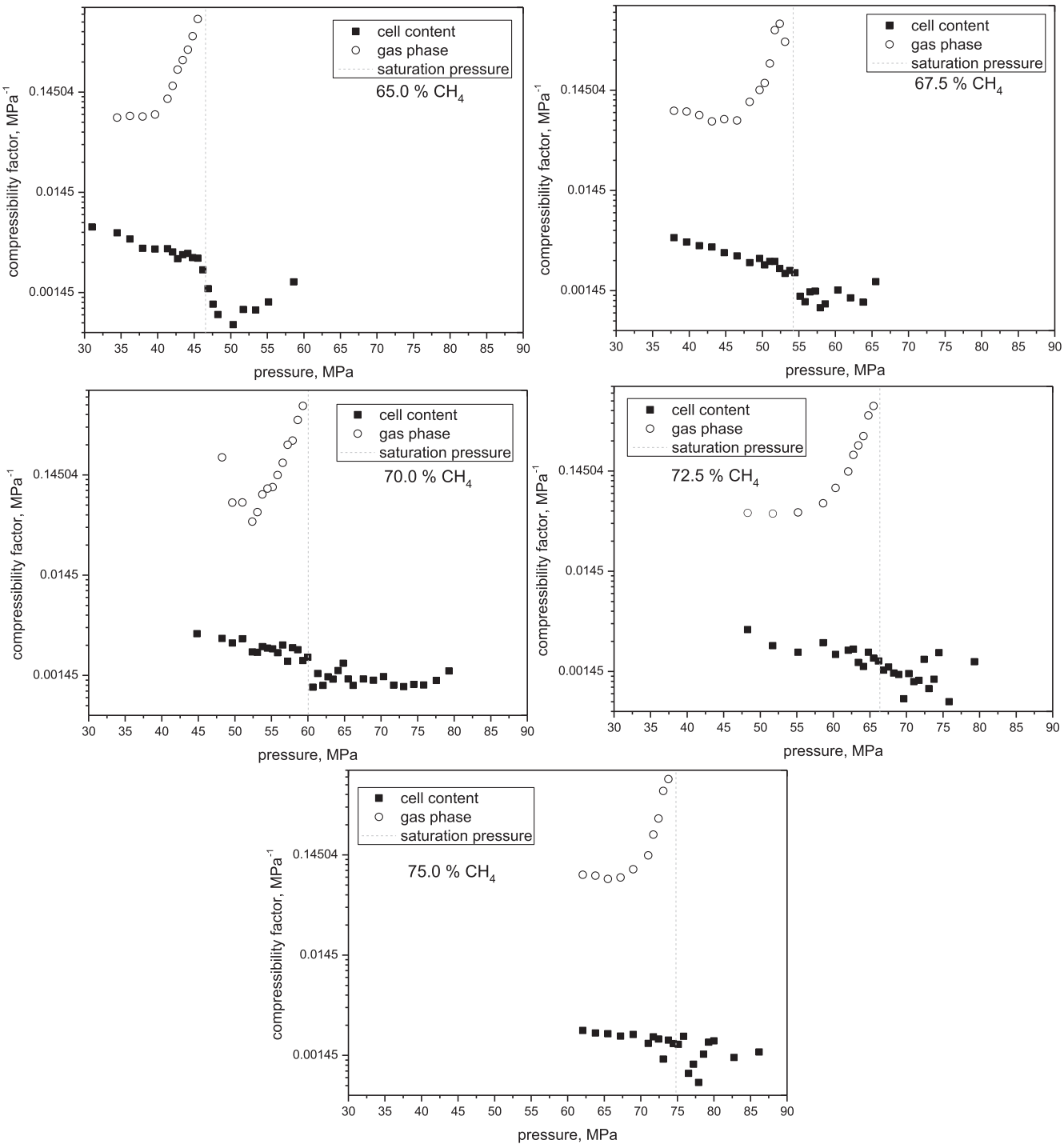

Fig. 3. Saturation pressure and isothermal compressibility for the overall system and the gas phase after the bubble point for crude oil and methane mixtures.

i.e., onset pressure regions, stability, morphology, and dissolution, especially for phase transitions above the bubble point pressure.

For all described above, phase behavior of dead crude oil + methane mixtures, at different gas (methane) ratio was studied in this work. The main objective is to better understand phase transition for reservoir fluids at high pressure condition. Phase boundaries were determined by using different analytical techniques: pressure-volume-temperature (PVT) measurements, coupled with a near infra-red (NIR) probe for solid detection system (SDS), together with a high-pressure microscopy (HPM) analysis. These techniques were used to identify liquid-vapor (LV) transitions and asphaltenes precipitation onset, as function of methane content. Asphaltene redissolution was also evaluated by system pressurization from pressures above asphaltenes onset precipitation to monophasic region.

2. Materials and methods

Phase equilibrium experiments of dead crude oil and methane systems were performed by intermediate of a synthetic method [42,43]. Crude oil and methane mixtures (65.0, 67.5, 70.0, 72.5 and 75.0 mol% of methane) were prepared, and their phase behavior was studied in a variable volume PVT cell. Two different tests were performed for each composition: a constant composition expansion (CCE) test, and an isothermal expansion for high pressure microscopy (HPM) analysis,

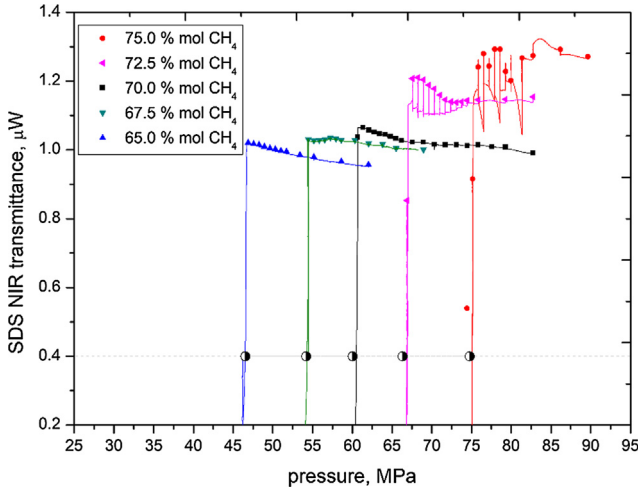

Fig. 4. NIR transmittance signal for equilibrium steps (solid symbols) and continue depressurization (lines) during CCE test. Saturation pressures marked (◑) for crude oil and methane mixtures.

detailed described in Sections 2.3 and 2.4. Both tests were made at reported reservoir temperature of 70 °C.

2.1. Crude oil sample

Dead crude oil sample was supplied by Petrobras. Table 1 depicts crude oil characterization, i.e., density, SARA (saturates, aromatics, resins and asphaltene) analysis, molar weight, and water content. Additionally, compositional analysis of the crude oil is presented in Table 2.

Density measurements were carried out by using an Anton Paar SVM 3000 viscodensimeter, based on a U-tube principle. Standard oils (CN-6773, Anton Paar) were used for calibration procedure, with an uncertainty of 0.0001 g/cm^3.

Asphaltene content was measured following a single stage n-heptane addition, as stated by Alboudwarej et al. [44] and described elsewhere [23]. Crudes SAR (saturates, aromatics, and resins) content was also determined by liquid chromatography fractionation, following ASTM D2007M procedure [45]. Analytical grade (> 99.8%) solvents (n-heptane, toluene, dichloromethane and methanol) supplied by Sigma-Aldrich were used. It is important to mention all chemicals were used with no further purification processes. Water content was determined by using a Karl-Fischer titration (Metrohm Brasil).

SARA fractionation of the crude oil was used to investigate its asphaltenes stability by intermediate of the Sepúlveda's Criterions, i.e., Qualitative-Quantitative Analysis (QQA), and Stability Cross Plot (SCP) test [46,47]. These asphaltene stability criteria are based in a series of relations between crude oil SARA fractions, the use of both tests is recommended to better results in asphaltene stability evaluation [46]. Details about the criterions are presented elsewhere [46,47].

2.2. PVT apparatus

A schematic diagram of the high-pressure system is presented in Fig. 1, with a detailed description made below.

PVT analysis have been performed by using Fluid-Eval cell (Vinci Technologies, France), with a maximum operational condition of 15,000 psi and 200 °C. The apparatus consists of a variable volume Hastelloy cell (accuracy volume measurements of 0.01 cm^3), embedded with a high-pressure pump (with a pressure accuracy of 0.1%). This system is also equipped with a magnetic driven stirrer for homogenization of the fluid sample.

Vapor phase could be visually identified through two sapphire windows placed at the top of the cell. Through these windows, volumetric measurements of the formed phase (with an accuracy of 0.02 cm^3) can be made using a video camera. Vinci VisionACq V1.5® software was used for image processing and volume calculation.

Near Infrared (NIR) transmittance through the crude sample was measured continuously during depletion using a Solid Detection System (SDS) provided by Vinci Technologies. A NIR laser source was connected to the PVT cell through an optic fiber. NIR transmittance was analyzed in the wavelength of 1,500 nm by an optical power meter with a minimal sensitivity of 1 pW.

HPM analysis were also performed for phase identification during the depressurization process. HPM cell consist of a high-pressure arrangement with two sapphires distanced by 100-µm where sample from the PVT flows through. HPM cell is connected between PVT cell and a high-pressure reservoir. Vinci HPM V1.0.11® software was used for micrograph analysis. From these analyses, it could be possible to detect the presence of particles, their counting, along with their size, with a minimal detection of 1 µm diameter.

2.3. PVT sample preparation and CCE test

Crude oil and gas were precisely introduced to the PVT cell, previously vacuumed at 1 kPa, by using high-pressure syringe pumps. Firstly, a volume of crude oil (80.00 mL) was injected in the PVT cell, at 40.0 °C and 690 kPa. Secondly, a required amount of methane (White Martins, 99.995 wt%) was injected by using a Teledyne Isco 260D syringe pump at 13.79 MPa (volume accuracy 0.01 cm^3). Gas temperature during injection procedure was controlled by intermediate of the cooling jacket of the syringe pump, by using a PolyScience AD07R-40 chiller, at 20.0 °C.

Temperature and pressure during injection were monitored to calculate the mass amount of each fluid introduced in the PVT cell. Density and molecular mass of crude oil were previously determined, as described in Table 1. Methane density was taken from NIST REFPROP V7 database (112.17 kg/m^3 at 20.0 °C and 13.79 MPa).

After the desired amount of crude oil and gas were injected to the PVT, the cell content was continuously stirred and pressurized with a rate of 415 kPa/min (60 psi/min) until at least 14 MPa above the bubble point. It was kept under stirring, at least, 12 h before the CCE test.

CCE test was performed by a controlled depressurization following equilibrium steps until at least 20 MPa below the detection of first bubbles. Depressurization steps were kept at 3400 kPa for pressures far from bubble point; and 690 kPa for pressures near the bubble point. Depressurization rate between equilibrium steps was 208 kPa/min (30 psi/min), at a minimal equilibrium time of 15 min. After this time, a three parameter criterium was adopted to ensure equilibrium was achieved, as follow: no variations on pressure higher than 35 kPa; 0.03 cm^3 of volume change; and, 1.0 °C temperature variation for at least 5 min. Only when this criterium is attained, pressure, temperature and volume values are taking by intermediate of a data acquisition software (AppliLab). It is important to mention that for each depressurization step, the system was stirred constantly. On the other hand, equilibrium steps were taken without stirring.

Phase transitions were identified by intermediate of three different techniques, as follow: (i) pressure-volume (PV curve) slope variation against pression [4,12]; (ii) visual identifications; and, (iii) variations on sample NIR transmittance [27,48]. For instance, bubble point pressure was determined by the changing on the slope for PV curves [4,12]. Visual identification of the first bubbles was recorded by the camera located in front of sapphire windows in the head cell. This analysis was important to the confirmation of the saturation pressure. Gas phase volume was determined by using the coupled camera. From these data, isothermal compressibility for the gas phase was also calculated. Monophasic isothermal compressibility at high pressures was determined by volumetric measurements form PVT embedded pump. Relative volume was calculated by dividing system volume (at each

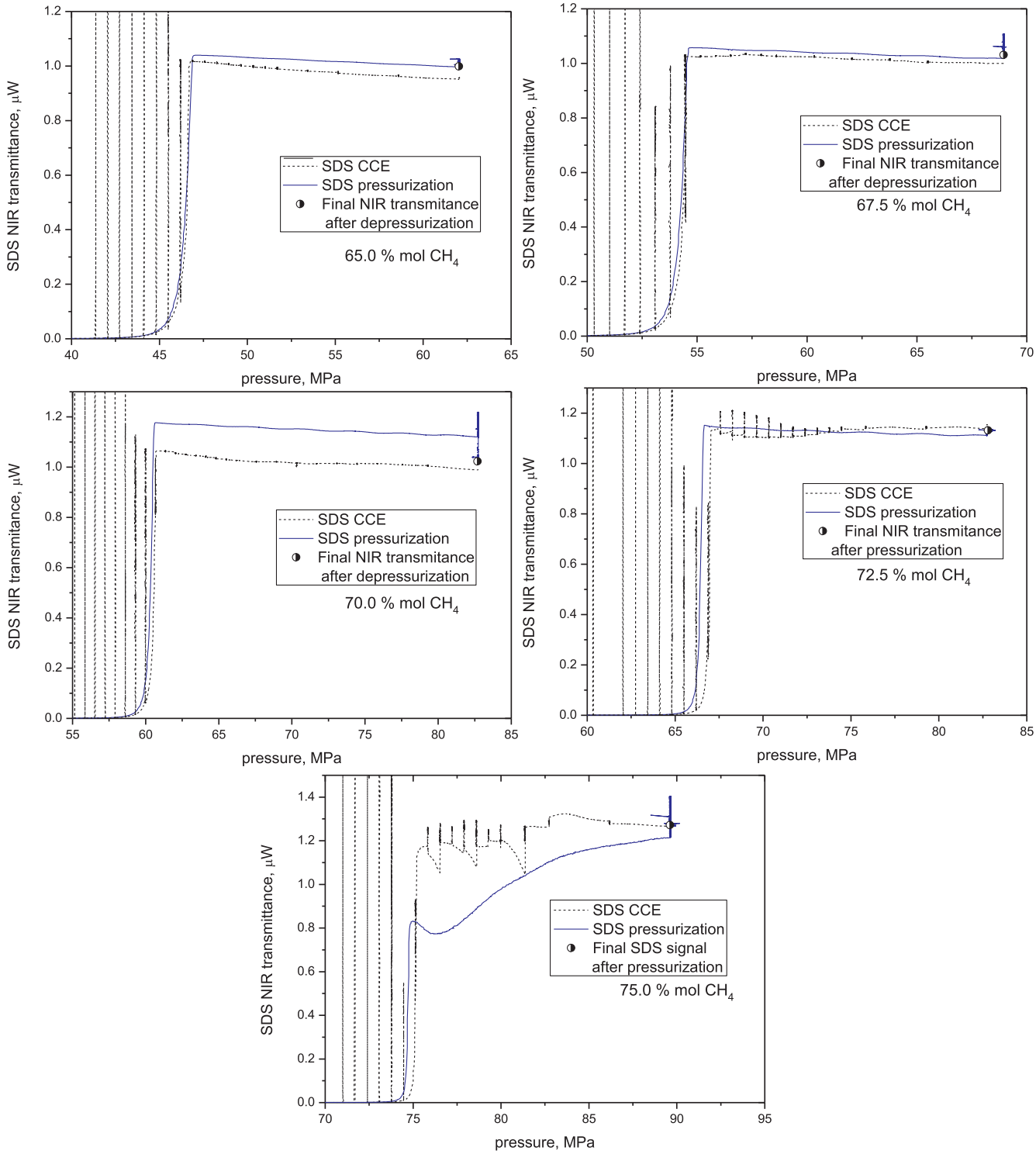

Fig. 5. NIR transmittance comparison during CCE and system re-pressurization for all crude oil and methane mixtures (65.0, 67.5, 70.0, 72.5, and 75.0 methane mol %).

equilibrium step) by the interpolated volume at the saturation pressure.

NIR transmittance were recorded continuously during depressurization and also at the equilibrium stages. It is important to state that NIR transmittance at saturation pressure is close to zero (10^{-8} W). Nevertheless, above bubble point pressure, a decreasing in NIR transmittance, could be related to solid formations, e.g., asphaltene onset pressure (AOP) [27,48].

After the last stage of equilibrium, the entire system was re-pressurized (at a rate of 415 kPa/min) to get the initial pressure of the test. After that, the system remains at rest during at least 12 h under stirring (750 rpm). Next, NIR transmittance before and after recombination was compared to assure the return to initial state. This sample was used then for isothermal depressurization HPM analysis.

2.4. Isothermal depressurization HPM analysis

Isothermal depressurization HPM analysis was conducted under a depressurization ramp of 208 kPa/min and equilibrium steps of 5 min.

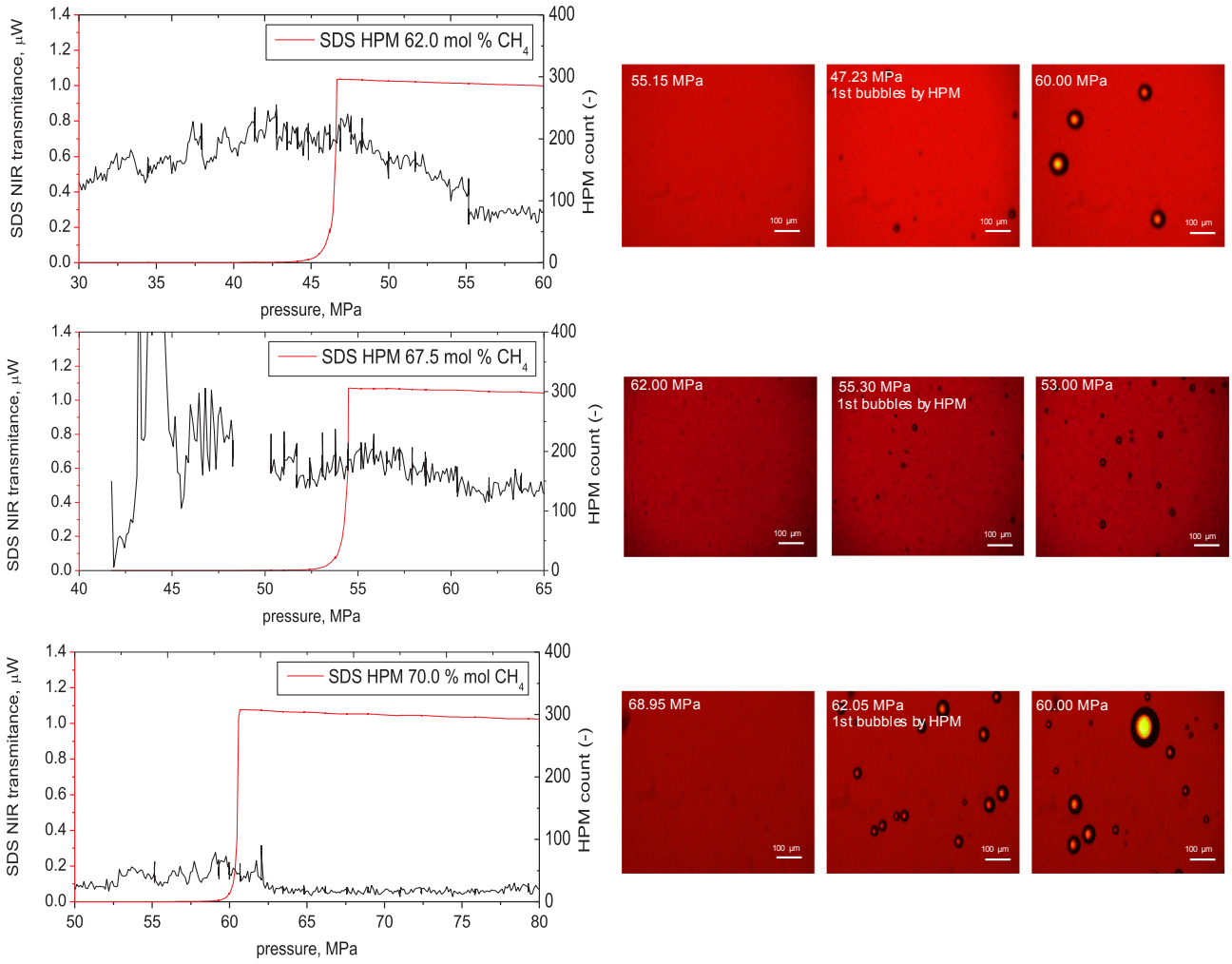

Fig. 6. NIR transmittance, HPM particle count and micrographs for crude oil and methane mixtures with 65.0, 67.5 and 70.0 methane mol% during HPM test.

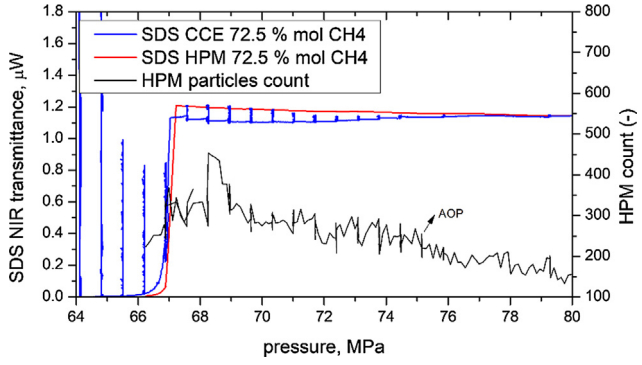

Fig. 7. NIR transmittance and HPM particle count for 72.5 methane mol% crude oil and methane mixture during HPM test.

Simultaneously, a flowrate of 0.1 cm^3/min was set in the syringe pump to flow fresh fluid from the PVT cell to the HPM cell. During the depressurization and equilibrium steps, phase formation, e.g. asphaltenes, were identified by particle count, aggregates size and relative coverage area, by using microscope camera and Vinci HPM V1.0.11® software. Micrographs were taken every 2 s. NIR transmittance measurements in the PVT cell during HPM test were also registered during both depletion and equilibrium steps.

Asphaltenes phase behavior were also evaluated in terms of dissolution by repressurizing the system from the AOP to the monophasic pressure. Pressurization was made by increasing PVT pressure with the HPM connected, at a rate of 415 kPa/min.

3. Results and discussion

3.1. CCE tests results

Relative volumes against pressure for all the crude oil + methane systems are depicted in Fig. 2. From these curves, saturation pressure was determined from the inflection point of the relative volume. It was observed that increasing methane molar content this inflection point is less evident, as expected. For methane compositions of 72.5 and 75.0 mol%, PV curve plots show a continuous shape, with no clear discontinuity [49]. For this reason, bubble point pressure is better determined by both visual observation of the first bubbles in the cell sapphire windows and by the steep decline of SDS NIR signal.

Compressibility calculation of each measured phase are presented in Fig. 3. Overall compressibility was directly calculated from the volumetric measurements of the cell content. These measurements are coincident to the monophasic compressibility at pressures above the saturation pressure. Below saturation pressure, two different compressibilities were calculated, one from the gas phase, obtained from frontal camera; and, another from volumetric behavior of the embedded pump. From these data, it could be observed a compressibility difference over 100-fold for the gas phase compared to the dense phase. This difference in compressibility confirms the measured bubble point and denotes the LV equilibrium for all the systems. It was

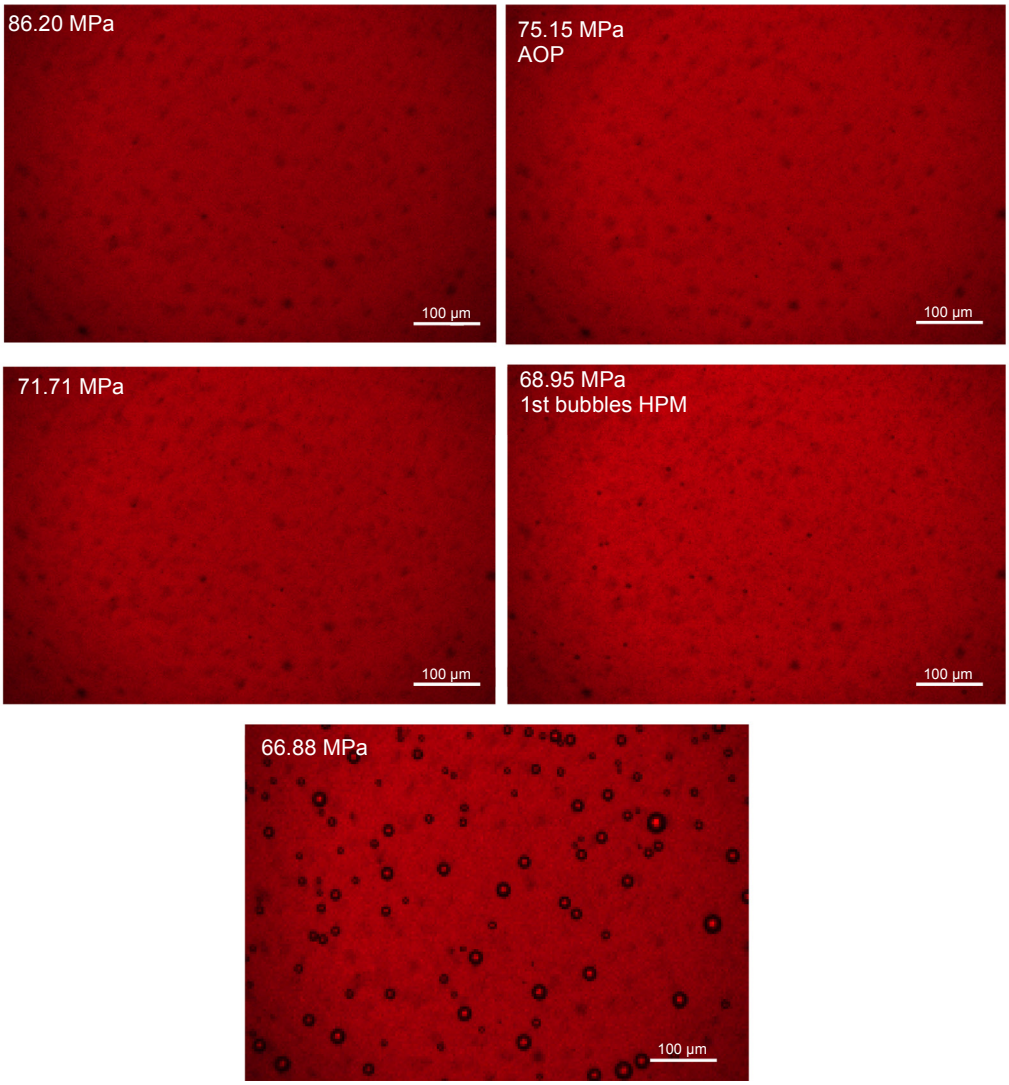

Fig. 8. Micrographs for 72.5 methane mol% mixture with crude oil during HPM test.

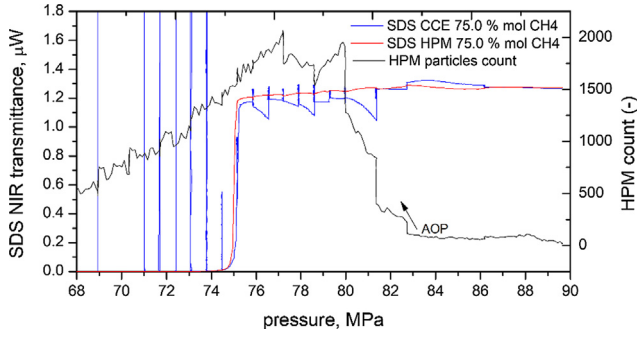

Fig. 9. NIR transmittance and HPM particle count for 75.0 methane mol% mixture with crude oil during HPM test.

observed that as methane content increases, the overall system compressibility variation becomes less evident, when saturation pressure is reached. For systems above 70 mol% of methane, the identification of the bubble point pressure was possible by means of a visual observation of the cell content and the NIR transmittance response.

Fig. 4 shows NIR signal measurements for equilibrium steps and the continue measurement during system depletion. It can be noted that a sharp NIR transmittance reduction was attained when bubble point was reached. It could be related to the bubbles formation leading to a high laser dispersion or density changes in the continuous oil phase that contributes to the increase of sample absorbance [27,48]. For system composition below 70 mol% of methane, a monotonic increase in NIR transmittance was detected during depletion until the saturation pressure. This behavior could be related to the reduction of the system density due to the depressurization. For systems with higher methane content, NIR transmittance variations were detected indicating a possible phase transition at pressure above the bubble point. This variation is normally related to asphaltenes when the AOP was reached. Nevertheless, for mixtures with high methane content, phase transition occurs at higher pressures, possibly due to solvency variation for asphaltenes [9]. NIR transmittance oscillation for 72.5 and 75.0 methane mol% were observed under stirring, between equilibrium steps, probably indicating a segregation process of the phase formed. Additionally, it could be observed that, during the equilibration of the stages, when PVT cell stirrer is turn off, NIR transmittance signal increases. These observations could indicate that the formed phase may aggregate and decant by gravity when system is not stirred, leaving the NIR laser path and consequently the SDS detection zone.

NIR transmittance signal comparison between sample depletion and repressurization process is shown in Fig. 5. It was noticed that all systems required a stabilization time to reach the initial transmittance, possible due to the delay in phase equilibrium caused by mass transfer limitations. For mixtures with methane content below 70.0 mol%,

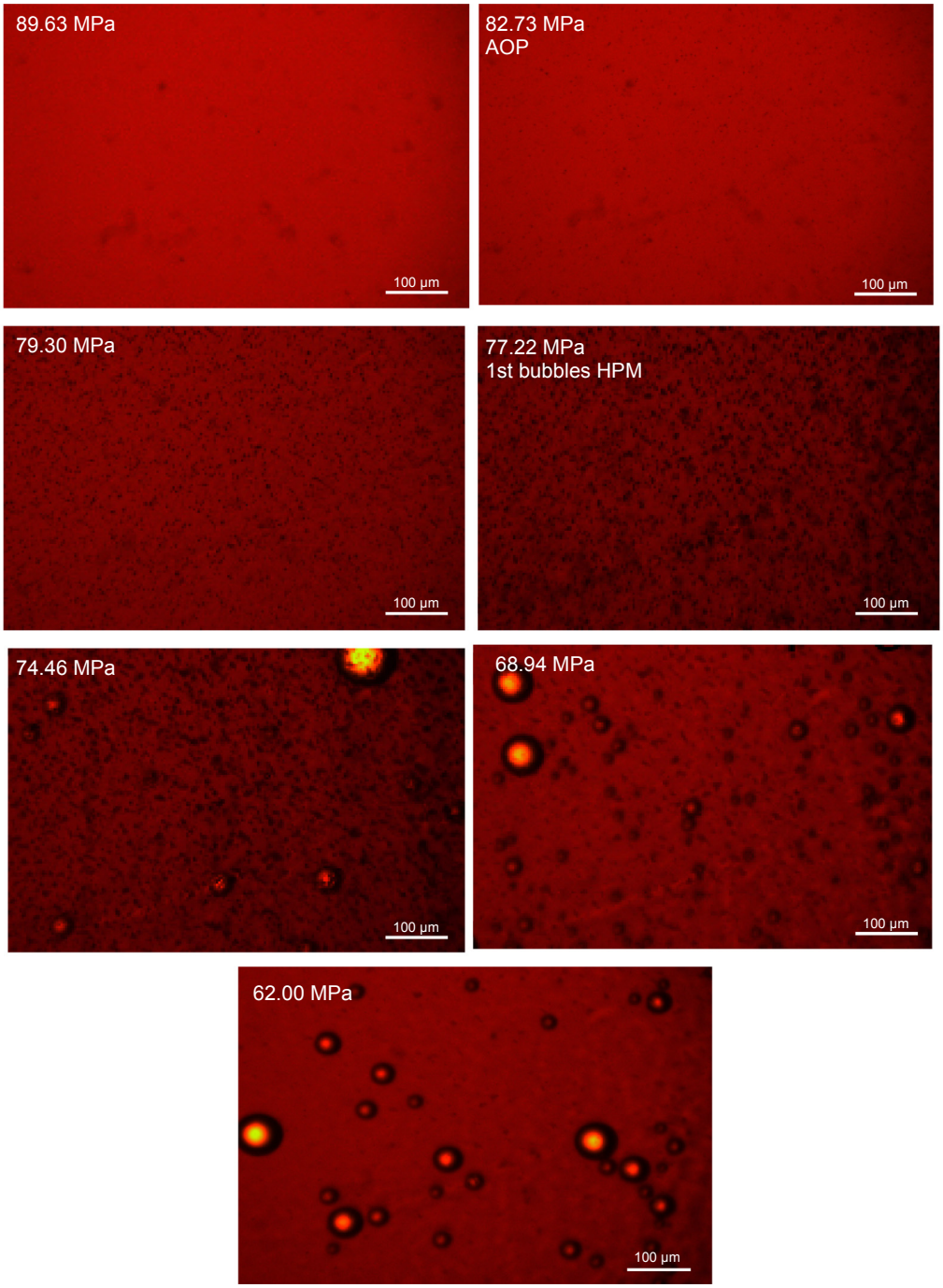

Fig. 10. Micrographs for 75.0 methane mol% mixture with crude oil during HPM test.

systems without apparent AOP, NIR transmittance was higher during recompression, and then decrease to the initial value after the equilibration time (at least 12 h). Samples NIR transmittance could be related inversely with density [27,48], and the decreasing of NIR transmittance after the stabilization time could indicate the stabilization in mixture density until reach equilibrium. Nevertheless, for systems with higher methane content, 72.5 and 75.0 mol%, NIR transmittance were lower during the pressurizing process and could be related to dispersed solids or heavy phase, like asphaltenes. After equilibration time, NIR transmittance reaches initial CCE NIR value. It important to mention, that no considerable hysteresis was detected for asphaltenes solubilization after the pressurizing process.

3.2. Isothermal depressurization HPM results

It is important to emphasize that all NIR transmittance data were investigated by HPM test in order to corroborate the phase transitions observation, described in the last Section. NIR transmittance, HPM particle count and micrographs for crude oil mixtures with 65.0, 67.5 and 70.0 methane mol% were present in Fig. 6. It was noted that NIR transmittance behaviors in the same way of CCE test. It means, with a monotonal increase during depletion until reach bubble point pressure. Micrographs analysis can confirm that there is any asphaltenes precipitation, no particles appearing were detected during depletion. Only LV transition is observed when saturation pressure was attained, with a maximum HPM count. It is important to mention that the constant response of SDS and HPM during depletion, i.e., constant particles count,

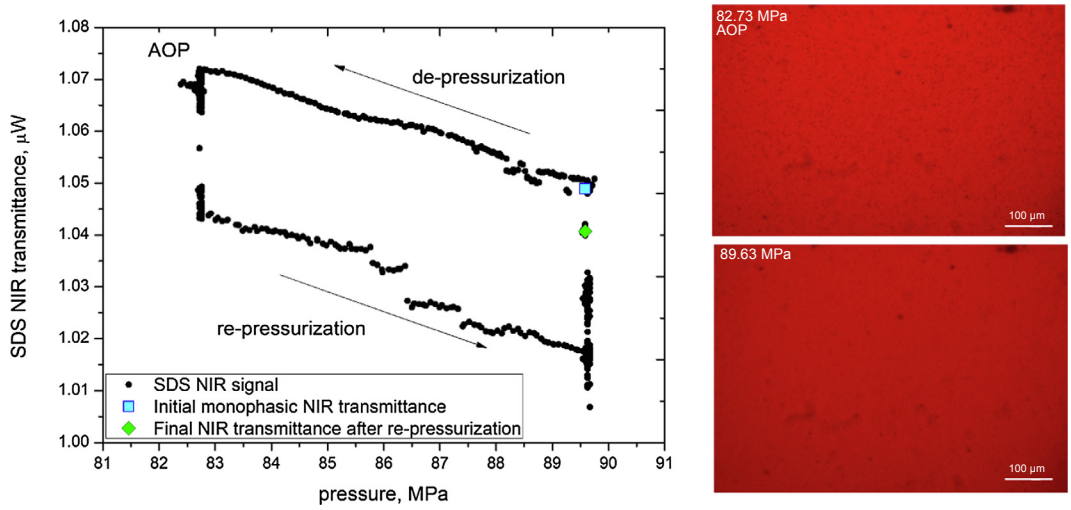

Fig. 11. SDS variation during AOP-monophasic pressurization test and micrographs for from pressures above the AOP to monophasic condition, for 75.0 methane mol% mixture with crude oil.

Table 3
Saturation pressure and AOP determined for the evaluated system of methane and dead crude oil at reservoir condition (70 °C).

methane content, % mol	CCE saturation pressure, MPa	AOP, MPa
65.0	46.5	–
67.5	54.2	–
70.0	60.1	–
72.5	66.3	75.2
75.0	74.8	82.7

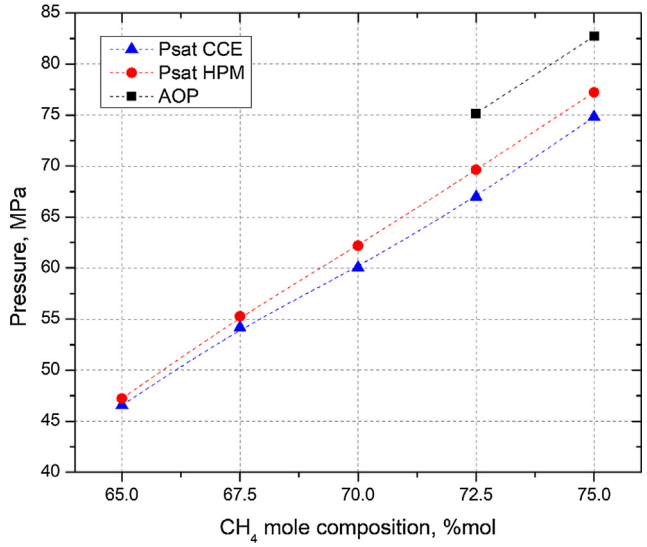

Fig. 12. P-composition diagram for methane and crude oil mixtures at reservoir conditions (70 °C).

no observation of particulate appearing, and SDS monotonal behavior, allows to confirm the absence of any other phases at pressure above the bubble point pressure. The difference on particle count between the systems could be associated with the initial estate of the HPM sapphire windows that represent a base line for each analysis.

Moreover, for these systems bubble point maximum difference obtained by using CCE and HPM was observed for 70.0 methane mol%, with a value of 2.05 MPa, with a 3.42% difference. It is interesting to remember that bubble point from CCE is always lower than HPM analysis. These differences could be associate to the accuracy techniques. During HPM test, the systems depletion is performed continuously, in difference with the equilibrium steps considered in CCE analysis. It has been reported in the literature that the depressurization rate could have influence in the bubble point pressure [50], and it could be related with the difference obtained by the two methods. It is expected that the CCE results were more accurate, by the consideration of the equilibrium steps during depletion [50]. The approximate error for the bubble pressure points determination, by intermediate of each technique, is within 100 psi (0.69 MPa).

Figs. 7–10 present HPM results for systems with higher methane content (72.5 and 75.0 mol%). It can be seen that micrographs and particles count confirm the appearance of another phase. This result is in accordance to SDS NIR transmittance, where there is a decrease on this signal when phase transition is observed. Fig. 7 shows SDS NIR transmittance along with HPM count for the system with 72.5 methane mol %. It is shown that there is an increase in HPM count during depletion, at the same pressure (75.15 MPa) SDS NIR decreases in the CCE test. This event could be related to a phase transition. It could be associated with asphaltenes (aggregation or flocculation) that contribute to decrease NIR transmittance. Likewise, Fig. 8 shows the formation of a fine dispersed phase, around 75.15 MPa. This phase shows no tendency to aggregate to form clusters. Also, it is remarkable that the phase disappeared entirely when the system reached bubble point pressure. Although asphaltenes are recognized to form fractal aggregates or flocs [33], micrographs do not show any fractal agglomeration.

Same behavior was obtained for 75.0 methane mol% system, as presented in Figs. 9 and 10. Nevertheless, phase transition event was more evident, for HPM test, even for SDS analysis. Fig. 9 depicts a sharp increase in HPM particles count. Once again, SDS NIR transmittance is in accordance to HPM results, i.e., SDS signal decrease at the same pressure where phase transition was detected by HPM test. Fig. 10 shows that this phase is characterized by form a fine particulate dispersed phase with no fractal aggregates despite higher particles count. Additionally, it was observed that when near saturation pressure was reached, there is a decreasing in fines asphaltenes particles. It is important to mention that this behavior was also observed for crude oils with no problems of asphaltenes precipitations [33,51]. Also, residual asphaltenes deposits in the sapphire until gradually dissolve with pressure decreasing. It is well known that crude oil properties, as low content of asphaltenes and high resins/asphaltene ratio, could contribute to the no asphaltenes aggregation and fine dispersion formation.

Moreover, stability of the asphaltenes could be associated with this no typical low aggregation and fine dispersion formation, observed in the micrographs. The stability could be verified using models that take

in account crude oil composition, based in SARA fractionation [46,47,52]. It has been reported that combined Sepúlveda's criterions, i.e., Quantitative-Qualitative analysis (QQA), and Stability Cross Plot (SCP), results in better prediction of asphaltene stability for crude oils [46,47]. When QQA and SCP method was applied, based on SARA composition of the used crude oil presented in Table 1, stable asphaltenes were predicted by both methods. The crude oil properties and the resulted asphaltene stability, could be related with the observed fine dispersion, low aggregation and fast dissolution of the particulate observed by the HPM.

In order to better understand these atypical results showed for systems with higher methane content (72.5 and 75.0 methane mol%), a new experiment has been done for the system with 75.0 methane mol%. A depressurization until AOP and then a compression until monophasic condition, as showed in Fig. 11. This figure presents the variation of SDS signal when system is depressurized to the AOP from the monophasic condition, and also compared with the SDS response when compressed. During the expansion, SDS signal increases due to the reduction in system density until the AOP was reached and the signal sharply decrease by particles interference. After 5 min, a micrograph was taken and it shows a fine dispersion, as described previously. After that, the system was repressurized until initial monophasic condition. During this compression, it was observed a decreasing in SDS signal that could be related to the increasing on the system density, until the monophasic pressure was reached. At this point, SDS signal recovers almost the original NIR transmittance, i.e., 1.4 μW vs 1.5 μW at the beginning of the test after the equilibration time. With less than 5 min of equilibration time, no asphaltenes were detected by HPM as one can note in the Fig. 11. Redissolution of the asphaltenes appears to be achieved with no kinetic restrictions. Although reports about slow redissolution of asphaltenes [27,28,33], the observed asphaltenes behavior support a thermodynamic phase transition with specific dependence of system states variables.

In summary, phase transitions (saturation pressure and AOP) for the system crude oil + methane at different methane content were listed in Table 3. Also, a pressure against composition diagram is presented in Fig. 12. From these data, it could be state that there is a slightly different on saturation pressure obtained by two different methods. Nevertheless, these results are in a good agreement between them. In addition, there is an increasing in saturation pression with the increasing on methane content, as expected. For the higher methane content systems (72.5 and 75.0 methane mol%), phase transition was observed with the formation of fine non-aggregate fine particles.

4. Conclusions

Brazilian pre-salt crude oil phase transitions were studied by intermediate of the addition of methane (from 65.0 to 75.0 methane mol %). Pressure-volume curves show a slight phase transition, by increasing methane molar content, along with the increasing of saturation pressure. For systems with higher methane molar content (72.5 and 75.0 methane mol %) a phase transition was detected by CCE test and HPM analysis. CCE test shows a SDS NIR transmittance variation during phase transition that could be associate with asphaltenes, that was confirmed by HPM analysis. This phase is characterized as a fine non-aggregate particles, with no fractal geometry. Asphaltenes solubility test reveals that there is a dissolution phenomenon of these particulate phase, with no hysteresis in NIR transmittances during depletion and compression cycling. This behavior could indicate a pure thermodynamic phase transition, with diminutive kinetic restriction for asphaltenes dissolution.

Acknowledgments

Financial support by REPSOL-Sinopec, Petrobras and The Brazilian National Agency of Petroleum, Natural Gas and Biofuels (ANP) are appreciated. The authors acknowledge to Petrobras for logistics and permissions in crudes samples supplying. The authors thank the discussions and technical support exchanged with Flow Assurance Group by Petrobras Cenpes.

References

[1] Aquino-Olivos MA, Grolier J-PE, Randzio SL, Aguirre-Gutiérrez AJ, García-Sánchez F. Determination of the asphaltene precipitation envelope and bubble point pressure for a Mexican crude oil by scanning transitiometry. Energy Fuels 2013;27:1212–22. https://doi.org/10.1021/ef301449e.
[2] Al Ghafri SZS, Forte E, Maitland GC, Rodriguez-Henríquez JJ, Trusler JPM. Experimental and Modeling study of the phase behavior of (methane + CO2 + water) mixtures. J Phys Chem B 2014;118:14461–78. https://doi.org/10.1021/jp509678g.
[3] Shaw JM, deLoos TW, Arons JdS. An explanation for solid-liquid-liquid-vapour phase behaviour in reservoir fluids. Pet Sci Technol 1997;15:503–21. https://doi.org/10.1080/10916469708949672.
[4] Johnston KA, Schoeggl FF, Satyro MA, Taylor SD, Yarranton HW. Phase behavior of bitumen and n-pentane. Fluid Phase Equilib 2017;442:1–19. https://doi.org/10.1016/j.fluid.2017.03.001.
[5] Gonzalez DL, Ting PD, Hirasaki GJ, Chapman WG. Prediction of asphaltene instability under gas injection with the PC-SAFT equation of state. Energy Fuels 2005;19:1230–4. https://doi.org/10.1021/ef049782y.
[6] Katz DL, Firoozabadi A. Predicting phase behavior of condensate/crude-oil systems using methane interaction coefficients. J Pet Technol 1978;30:1649–55. https://doi.org/10.2118/6721-PA.
[7] Mehrotra AK, Svrcek WY. Correlation and prediction of gas solubility in cold lake bitumen. Can J Chem Eng 1988;66:666–70. https://doi.org/10.1002/cjce.5450660420.
[8] Cao M, Gu Y. Temperature effects on the phase behaviour, mutual interactions and oil recovery of a light crude oil–CO2 system. Fluid Phase Equilib 2013;356:78–89. https://doi.org/10.1016/j.fluid.2013.07.006.
[9] Cardoso FMR, Carrier H, Daridon J-L, Pauly J, Rosa PTV. CO_2 and temperature effects on the asphaltene phase envelope as determined by a quartz crystal resonator. Energy Fuels 2014;28:6780–7. https://doi.org/10.1021/ef501488d.
[10] Kia A, Sarlak AR, Tabari AH, Afkan SB, Keshavarz M, Maddah H. Experimental and theoretical study of phase behavior for live oil during CO_2 EOR process. Pet Sci Technol 2017;35:451–6. https://doi.org/10.1080/10916466.2016.1201488.
[11] Long B, Chodakowski M, Shaw JM. Impact of liquid-vapor to liquid–liquid–vapor phase transitions on asphaltene-rich nanoaggregate behavior in athabasca vacuum residue + pentane mixtures. Energy Fuels 2013;27:1779–90. https://doi.org/10.1021/ef301475f.
[12] Agrawal P, Schoeggl FF, Satyro MA, Taylor SD, Yarranton HW. Measurement and modeling of the phase behavior of solvent diluted bitumens. Fluid Phase Equilib 2012;334:51–64. https://doi.org/10.1016/j.fluid.2012.07.025.
[13] Dini Y, Becerra M, Shaw JM. Phase behavior and thermophysical properties of Peace River bitumen + propane mixtures from 303 K to 393 K. J Chem Eng Data 2016;61:2659–68. https://doi.org/10.1021/acs.jced.6b00034.
[14] AlQuraishi AA. Determination of crude oil saturation pressure using linear genetic programming. Energy Fuels 2009;23:884–7. https://doi.org/10.1021/ef800878h.
[15] Tavakkoli M, Panuganti SR, Taghikhani V, Pishvaie MR, Chapman WG. Precipitated asphaltene amount at high-pressure and high-temperature conditions. Energy Fuels 2014;28:1596–610. https://doi.org/10.1021/ef401074e.
[16] Araújo CBK, Capitelli FO, Rajagopal K, Corazza ML, Ndiaye PM. Phase behavior of Brazilian stock tank oil and carbon dioxide at reservoir conditions: experiments and thermodynamic modeling. J Pet Explor Prod Technol 2016;6:39–44. https://doi.org/10.1007/s13202-015-0165-y.
[17] Speight JG. Petroleum asphaltenes – Part 1: Asphaltenes, resins and the structure of petroleum. Oil Gas Sci Technol 2004;59:467–77. https://doi.org/10.2516/ogst:2004032.
[18] Díaz OC, Modaresghazani J, Satyro MA, Yarranton HW. Modeling the phase behavior of heavy oil and solvent mixtures. Fluid Phase Equilib 2011;304:74–85. https://doi.org/10.1016/j.fluid.2011.02.011.
[19] Maqbool T, Srikiratiwong P, Fogler HS. Effect of temperature on the precipitation kinetics of asphaltenes. Energy Fuels 2011;25:694–700. https://doi.org/10.1021/ef101112r.
[20] Calles JA, Dufour J, Marugán J, Peña JL, Giménez-Aguirre R, Merino-García D. Properties of asphaltenes precipitated with different n-alkanes. A study to assess the most representative species for modeling. Energy Fuels 2008;22:763–9. https://doi.org/10.1021/ef700404p.
[21] Rogel E, Moir M. Effect of precipitation time and solvent power on asphaltene characteristics. Fuel 2017;208:271–80. https://doi.org/10.1016/j.fuel.2017.06.116.
[22] Ramos AC da S, Rolemberg MP, de Moura LGM, Zilio EL, dos Santos M de FP, González G. Determination of solubility parameters of oils and prediction of oil compatibility. J Pet Sci Eng 2013;102:36–40. https://doi.org/10.1016/j.petrol.2013.01.008.
[23] Romero Yanes JF, Feitosa FX, do Carmo FR, de Sant'Ana HB. Paraffin effects on the stability and precipitation of crude oil asphaltenes: experimental onset determination and phase behavior approach. Fluid Phase Equilibria 2018;474:116–25. https://doi.org/10.1016/j.fluid.2018.07.017.
[24] Cao M, Gu Y. Oil recovery mechanisms and asphaltene precipitation phenomenon in immiscible and miscible CO2 flooding processes. Fuel 2013;109:157–66. https://

doi.org/10.1016/j.fuel.2013.01.018.
[25] Yonebayashi H, Al Mutairi AM, Al Habshi AM, Urasaki D. Dynamic asphaltene behavior for gas-injection risk analysis. SPE Reserv Eval Eng 2011;14:493–504. https://doi.org/10.2118/146102-PA.
[26] Zhang X, Pedrosa N, Moorwood T. Modeling asphaltene phase behavior: comparison of methods for flow assurance studies. Energy Fuels 2012;26:2611–20. https://doi.org/10.1021/ef201383r.
[27] Hammami A, Phelps CH, Monger-McClure T, Little TM. Asphaltene precipitation from live oils: an experimental investigation of onset conditions and reversibility. Energy Fuels 2000;14:14–8. https://doi.org/10.1021/ef990104z.
[28] Chaisoontornyotin W, Bingham AW, Hoepfner MP. Reversibility of asphaltene precipitation using temperature-induced aggregation. Energy Fuels 2017;31:3392–8. https://doi.org/10.1021/acs.energyfuels.6b02344.
[29] Hirschberg A, deJong LNJ, Schipper BA, Meijer JG. Influence of temperature and pressure on asphaltene flocculation. Soc. Pet. Eng. J. 1984;24:283–93. https://doi.org/10.2118/11202-PA.
[30] Cimino R, Correra S, Sacomani PA, Carniani C. Thermodynamic modelling for prediction of asphaltene deposition in live oils, in: Society of Petroleum Engineers, 1995. doi: 10.2118/28993-MS.
[31] Leontaritis KJ. Asphaltene deposition: a comprehensive description of problem manifestations and modeling approaches, in: Society of Petroleum Engineers, 1989. doi: 10.2118/18892-MS.
[32] Kawanaka S, Leontaritis KJ, Park SJ, Mansoori GA, Thermodynamic and colloidal models of asphaltene flocculation. In: Oil-Field Chem., American Chemical Society, 1989: pp. 443–458. doi: 10.1021/bk-1989-0396.ch024.
[33] Mohammadi S, Rashidi F, Mousavi-Dehghani SA, Ghazanfari M-H. Reversibility of asphaltene aggregation in live oils: qualitative and quantitative evaluation. J Chem Eng Data 2015;60:2646–54. https://doi.org/10.1021/acs.jced.5b00297.
[34] Vilas Bôas Fávero C, Maqbool T, Hoepfner M, Haji-Akbari N, Fogler HS. Revisiting the flocculation kinetics of destabilized asphaltenes. Adv Colloid Interface Sci 2017;244:267–80. https://doi.org/10.1016/j.cis.2016.06.013.
[35] Rogel E, León O, Contreras E, Carbognani L, Torres G, Espidel J, et al. Assessment of asphaltene stability in crude oils using conventional techniques. Energy Fuels 2003;17:1583–90. https://doi.org/10.1021/ef0301046.
[36] Wang JX, Brower KR, Buckley JS. Observation of asphaltene destabilization at elevated temperature and pressure. SPE J 2000;5:420–5. https://doi.org/10.2118/67856-PA.
[37] Artola P-A, Pereira FE, Adjiman CS, Galindo A, Müller EA, Jackson G, et al. Understanding the fluid phase behaviour of crude oil: asphaltene precipitation. Fluid Phase Equilib 2011;306:129–36. https://doi.org/10.1016/j.fluid.2011.01.024.
[38] Hu R, Crawshaw JP, Trusler JPM, Boek ES. Rheology and phase behavior of carbon dioxide and crude oil mixtures. Energy Fuels 2017;31:5776–84. https://doi.org/10.1021/acs.energyfuels.6b01858.
[39] Vargas FM, Gonzalez DL, Hirasaki GJ, Chapman WG. Modeling asphaltene phase behavior in crude oil systems using the perturbed chain form of the statistical associating fluid theory (PC-SAFT) equation of state. Energy Fuels 2009;23:1140–6. https://doi.org/10.1021/ef8006678.
[40] Ting PD, Hirasaki GJ, Chapman PWG. Modeling of asphaltene phase behavior with the SAFT equation of state. Pet Sci Technol 2003;21:647–61. https://doi.org/10.1081/LFT-120018544.
[41] AlHammadi AA, Vargas FM, Chapman WG. Comparison of cubic-plus-association and perturbed-chain statistical associating fluid theory methods for modeling asphaltene phase behavior and pressure–volume–temperature properties. Energy Fuels 2015;29:2864–75. https://doi.org/10.1021/ef502129p.
[42] Al Ghafri SZ, Maitland GC, Trusler JPM. Experimental and modeling study of the phase behavior of synthetic crude oil + CO2. Fluid Phase Equilibria 2014;365:20–40. https://doi.org/10.1016/j.fluid.2013.12.018.
[43] Gui X, Wang W, Gao Q, Yun Z, Fan M, Chen Z. Measurement and correlation of high pressure phase equilibria for CO2 + alkanes and CO2 + crude oil systems. J Chem Eng Data 2017;62:3807–22. https://doi.org/10.1021/acs.jced.7b00517.
[44] Alboudwarej H, Beck J, Svrcek WY, Yarranton HW, Akbarzadeh K. Sensitivity of asphaltene properties to separation techniques. Energy Fuels 2002;16:462–9. https://doi.org/10.1021/ef010213p.
[45] Kharrat AM, Zacharia J, Cherian VJ, Anyatonwu A. Issues with comparing SARA methodologies. Energy Fuels 2007;21:3618–21. https://doi.org/10.1021/ef700393a.
[46] Guzmán R, Ancheyta J, Trejo F, Rodríguez S. Methods for determining asphaltene stability in crude oils. Fuel 2017;188:530–43. https://doi.org/10.1016/j.fuel.2016.10.012.
[47] Kumar R, Voolapalli RK, Upadhyayula S. Prediction of crude oil blends compatibility and blend optimization for increasing heavy oil processing. Fuel Process Technol 2018;177:309–27. https://doi.org/10.1016/j.fuproc.2018.05.008.
[48] Lei H, Yang S, Qian K, Chen Y, Li Y, Ma Q. Experimental investigation and application of the asphaltene precipitation envelope. Energy Fuels 2015;29:6920–7. https://doi.org/10.1021/acs.energyfuels.5b01237.
[49] Amjad K, Ahsan SA, Sultan MA, Hegazy GM. Reservoir fluid identification – a case study of a near critical fluid from low permeability exploratory reservoir. In: Abu Dhabi Int. Pet. Exhib. Conf., Society of Petroleum Engineers, Abu Dhabi, UAE, 2016. doi: 10.2118/182946-MS.
[50] Zhou X, Yuan Q, Zeng F, Zhang L, Jiang S. Experimental study on foamy oil behavior using a heavy oil-methane system in the bulk phase. J Pet Sci Eng 2017;158:309–21. https://doi.org/10.1016/j.petrol.2017.07.070.
[51] Abutaqiya MIL, Sisco CJ, Wang J, Vargas FM. Systematic investigation of asphaltene deposition in the wellbore and near-wellbore region of a deepwater oil reservoir under gas injection. Part 1: Thermodynamic modeling of the phase behavior of polydisperse asphaltenes. Energy Fuels 2019. https://doi.org/10.1021/acs.energyfuels.8b03234.
[52] Yen A, Yin YR, Asomaning S. Evaluating asphaltene inhibitors: laboratory tests and field studies. In: Society of Petroleum Engineers, 2001. doi: 10.2118/65376-MS.